CHEMISTRY OF MATERIALS

Article

pubs.acs.org/cm

Lithiation and Delithiation Dynamics of Different Li Sites in Li-Rich Battery Cathodes Studied by *Operando* Nuclear Magnetic Resonance

Xiang Li,[†] Mingxue Tang,[†,‡] Xuyong Feng,[†] Ivan Hung,[‡] Alyssa Rose,[†] Po-Hsiu Chien,[†] Zhehong Gan,[‡] and Yan-Yan Hu*[,†,‡]

[†]Department of Chemistry and Biochemistry, Florida State University, Tallahassee, Florida 32306, United States

[‡]National High Magnetic Field Laboratory, 1800 East Paul Dirac Drive, Tallahassee, Florida 32310, United States

Supporting Information

ABSTRACT: Li in Li-rich cathodes mostly resides at octahedral sites in both Li layers (Li_{Li}) and transition metal layers (Li_{TM}). Extraction and insertion of Li_{Li} and Li_{TM} are strongly influenced by surrounding transition metals. pjMATPASS and *operando* Li nuclear magnetic resonance are combined to achieve both high spectral and temporal resolution for quantitative real time monitoring of lithiation and delithiation at Li_{Li} and Li_{TM} sites in Li_2MnO_3, $Li_{1.2}Ni_{0.2}Mn_{0.6}O_2$, and $Li_{1.2}Ni_{0.13}Mn_{0.54}Co_{0.13}O_2$ cathodes. The results have revealed that Li_{TM} are preferentially extracted for the first 20% of charge and then Li_{Li} and Li_{TM} are removed at the same rate. No preferential insertion or extraction of Li_{Li} and Li_{TM} is observed beyond the first charge. Ni and Co promote faster and more complete removal of Li_{TM}. The recovery of the removed Li is <60% for Li_{TM} and >80% for Li_{Li} upon first discharge. The study sheds light on the activity of Li_{Li} and Li_{TM} during electrochemical processes as well as their respective contributions to cathode capacity.

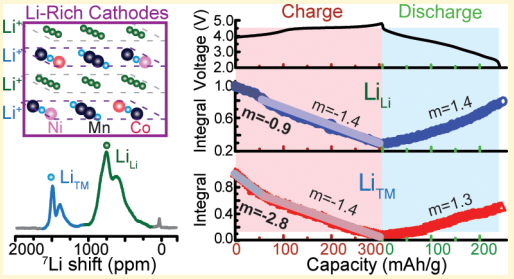

INTRODUCTION

The fast-growing demand for safe and low-cost energy storage technologies with high power and energy densities drives the continuous improvement of rechargeable Li-ion batteries (LIBs).[1,2] The capacities of LIBs are limited by cathodes. Layered manganese (Mn)-based Li-rich materials, namely $xLi_2MnO_3\cdot(1-x)LMO_2$ where M = Ni, Mn, or Co, represent the state of the art.[3−8] The structure of Li-rich compounds derives from that of layered $LiMO_2$ (hexagonal cell, space group $R\bar{3}m$) by a progressive Li^+ substitution for M^{3+} and charge compensation with an increased valence state of the remaining M elements.[9] Among them, Li-rich Li_2MO_3 exhibits a monoclinic O3-type structure with a space group of $C2/m$ to account for the distortion induced by the ordered distribution of the Mn^{4+}/Li^+ cations in the mixed $[Li_{1/3}Mn_{2/3}]O_2$ layer.[10,11] In Li_2MnO_3, Li ions are surrounded by six M atoms to form a honeycomb pattern. $Li_{1.2}Ni_{0.2}Mn_{0.6}O_2$ (LNMO) and $Li_{1.2}Ni_{0.13}Mn_{0.54}Co_{0.13}O_2$ (LNMCO) are solid solutions of Li_2MnO_3 and $LiMO_2$ (M = Mn, Ni, or Co). Li ions reside in both transition metal (TM) layers and Li layers, denoted as Li_{TM} and Li_{Li}, respectively, in this paper. Understanding the electrochemical reactivity of Li_{Li} and Li_{TM} in Li-rich cathodes and the associated impact of TMs will help the design of cathodes with high capacity. Li atoms are light and, thus, not easily detected with traditional diffreaction or electron microscopy approaches. In the early studies, Van der Ven and Ceder applied first-principles computations and Monte Carlo simulations on $LiNi_{0.5}Mn_{0.5}O_2$ to study the order rearrangement and Li extraction and insertion dynamics.[12] They found that at the beginning of charge, the Li ions in the transition metal layers were removed, freeing up tetrahedral sites that were then repopulated by lithium, and the tetrahedral Li required a high potential to be removed. Subsequently with a combination of neutron diffraction, *ex situ* ^{6}Li nuclear magnetic resonance (NMR), and density functional theory (DFT) calculations, Grey and co-workers[13] found that Li was extracted from both the TM and the Li layers for $LiNi_{0.5}Mn_{0.5}O_2$ in the early stages of charge, only a small amount of Li was left in the TM layer, and a large fraction of Li remained in tetrahedral sites, in general agreement with computational modeling.[14] Recently, Persson and co-workers performed detailed first-principles calculations on Li-excess Li_xMnO_3.[15,16] Their studies provided new insights into the electrochemical and structural stability of Li_xMnO_3. The formation energy calculations on Li_xMnO_3 structures predicted a sequence of extraction of Li from the thermodynamic perspective, which suggested that Li from the TM layer (2b sites) and partially from the Li layer (2c sites) can be extracted out first followed by Li at the 4h sites in the Li layer. It was also found that a sufficient number of vacancies in the Li layer promoted spontaneous migration of Li from the TM layer to the Li layer.[16] *In situ* monitoring of Li extraction and insertion under battery operating conditions is necessary to gain real time insights into the lithiation and delithiation dynamics of different Li sites. Recently, Meng et al. applied *operando* neutron diffraction (ND) to follow the dynamics of both Li and O atoms in Co- and Ni-containing Li-

Received: June 21, 2017
Revised: August 11, 2017
Published: September 18, 2017

Downloaded via FLORIDA STATE UNIV on July 18, 2024 at 19:00:11 (UTC).
See https://pubs.acs.org/sharingguidelines for options on how to legitimately share published articles.

© 2017 American Chemical Society

DOI: 10.1021/acs.chemmater.7b02589
Chem. Mater. 2017, 29, 8282−8291

rich NMC cathodes[17] and found that the Li extraction was mainly from Li layers. This finding was different from the prior computational and experimental studies of $LiNi_{0.5}Mn_{0.5}O_2$. The difference may be due to discrepancies in the characteristics between $LiNi_{0.5}Mn_{0.5}O_2$ and Li-rich NMC. Therefore, more detailed and comprehensive investigations are necessary to address the Li extraction and insertion dynamics at various Li sites in Li-rich cathodes with *operando* characterizations of high temporal resolution.

NMR has been shown to be a powerful tool for determining Li local environments[18−26] and their evolution during electrochemical operation.[27−37] Fermi contact interactions between unpaired electrons on Mn, Ni, Co, and Li are significantly different for Li_{Li} and Li_{TM}, which leads to well-separated resonances, with Li_{Li} typically resonating at 780 ppm and Li_{TM} at 1500 ppm in Li NMR spectra. This provides a means of clearly distinguishing Li_{Li} and Li_{TM}, using NMR. However, strong nuclear−electron dipolar interactions in LMO cathodes often lead to very large shift anisotropy and result in overlapping spinning sidebands (SSBs) in Li spectra, even under ultrafast magic-angle spinning (MAS) conditions.[18,34,38−48] This prevents accurate quantification of the (de)lithiation process. Because of a relatively smaller quadrupole moment of ^{6}Li compared to that of ^{7}Li, ^{6}Li NMR performed at fast MAS provides better resolution and, thus, is often preferred for quantitative studies of Li-rich cathodes in earlier investigations.[49] The results showed that only a small fraction (~7%) of the extracted Li_{TM} reinserted back into the TM layer. This is because certain tetrahedral Li is likely formed during charge and will block reinsertion of Li into TM layers upon discharge.[17,49] Although ^{6}Li MAS spectra can be used to quantify the (de)lithiation process *ex situ*, it requires complex sample treatments with expensive ^{6}Li isotope enrichment. Also as a result of the low sensitivity associated with ^{6}Li NMR (12.5 times lower than that of ^{7}Li), it is extremely challenging to perform *operando* characterizations.

To achieve a high spectral resolution for reliable quantification and a high sensitivity for high temporal resolution to follow the (de)lithiation process in real time, in this work we employ a combination of our previously developed NMR method, projection magic-angle turning and phase-adjusted sideband separation (pjMATPASS),[50] and *operando* ^{7}Li NMR. The pjMATPASS technique allows well-resolved resonances without interference from SSBs in ^{7}Li NMR spectra at a relatively low sample spinning frequency, which has been successfully demonstrated to achieve high-resolution spectra for pristine Mn-based paramagnetic cathodes.[50,51] Here, LMO cathodes at different states of charge are selected to perform pjMATPASS experiments *ex situ*. The high-resolution pjMATPASS spectra permit reliable quantification of different Li sites and tracking their evolution.

In addition, *operando* ^{7}Li NMR is also applied for the three aforementioned LMO cathodes, Li_2MnO_3, LNMO, and LNMCO. The parameters obtained from *ex situ* pjMATPASS NMR analysis are used to simulate ^{7}Li NMR spectra under static conductions, which allow robust quantitation of *operando* ^{7}Li NMR spectra. The combination of the high spectral resolution provided by pjMATPSS NMR and high sensitivity provided by ^{7}Li NMR allows quantitative *operando* characterization of Li_{Li} and Li_{TM} extraction and insertion dynamics in Li-rich cathode materials.

EXPERIMENTAL SECTION

Preparation of Materials. Li_2MnO_3 was synthesized using a solid-state reaction method from precursors Li_2CO_3 and $MnCO_3$ with a $Li_2CO_3/MnCO_3$ ratio of 1.05. The mixture of the precursors was ball-milled for 2 h, heated at 500 °C for 5 h, and then calcined at 700 °C for 24 h. $Li_{1.2}Ni_{0.2}Mn_{0.6}O_2$ (LNMO) was synthesized using a sol−gel method. All reagents (Sigma-Aldrich) were used as purchased. A stoichiometric amount of $CH_3COOLi{\cdot}2H_2O$ (99.999%), $(CH_3COO)_2Ni{\cdot}4H_2O$ (99.99%), $(CH_3COO)_2Mn{\cdot}4H_2O$ (99.99%), and citric acid (99%) were dissolved in distilled water at a molar ratio of 1.25:0.20:0.60:0.80. The temperature of the solution was kept at 85 °C to form a gel, and the pH value was maintained around 9 by adding NH_4OH(aq). The gel was preheated at 200 °C for 5 h, followed by annealing at 900 °C for 10 h. $Li_{1.2}Ni_{0.13}Mn_{0.54}Co_{0.13}O_2$ (LNMCO) was synthesized using the same procedure, except that a stoichiometric amount of $(CH_3COO)_2Co{\cdot}4H_2O$ (99.99%) was added. The phase purity of the Li_2MnO_3, LNMO, and LNMCO materials was determined via powder X-ray diffraction (XRD) (Figure S1).

Battery Fabrication and Electrochemistry. The synthesized Li_2MnO_3, LNMO, or LNMCO was mixed with polyvinylidene fluoride (PVDF) (Kynar Flex 2801 from Arkema) and conductive acetylene black [80:10:10 (w/w/w)]. The mixture was dispersed in *N*-methyl-2-pyrrolidone (NMP) and manually ground in an agate mortar for 30 min to form a homogeneous slurry. The slurry was cast onto an Al foam and Ti mesh for cathode preparations for *ex situ* (coin cell) and *operando* (bag cell) ^{7}Li NMR measurements, respectively. The cathodes were dried at 120 °C for 4 h under vacuum before assembling batteries in an argon-filled glovebox. The Li_2MnO_3, LNMCO, or LNMO cathode and Li metal anode were separated by a piece of porous glass microfiber (Whatman, type GF/D), soaked with the LP30 electrolyte, which contains 1 M $LiPF_6$ in ethylene carbonate and dimethyl carbonate [1:1 (w/w), Merck]. All cycled electrodes were washed three times with NMP to remove residual electrolyte.

***Ex Situ* ^{7}Li NMR.** ^{7}Li magic-angle spinning (MAS) NMR experiments were performed on a Bruker Avance III spectrometer in a 14.1 T magnetic field with a ^{7}Li Larmor frequency of 233.21 MHz. Electrodes were packed into 1.3 mm rotors and spun at a MAS rate of 50 kHz. The pjMATPASS pulse sequence[50] was employed to achieve high-resolution NMR spectra. The recycle delay was 0.3 s, and the 90° pulse length was 1.0 μs. LiCl(s) with a ^{7}Li chemical shift at 0 ppm was used as a reference.

***Operando* ^{7}Li NMR.** For *operando* NMR measurements, plastic bag cell batteries were assembled in an argon-filled glovebox and placed inside a home-built static NMR probe. ^{7}Li NMR spectra were recorded while the batteries were cycled at a rate of C/30, with theoretical capacities (C) of 458, 378, and 377 mAh/g (assuming all Li ions are completely extracted) used for Li_2MnO_3, LNMO, and LNMCO, respectively. All *operando* ^{7}Li NMR acquisitions were performed on a Bruker Avance I spectrometer in a 9.4 T magnetic field with a ^{7}Li Larmor frequency of 155.4 MHz. The ^{7}Li spectra were recorded using a spin echo sequence with a 90° pulse length of 2.6 μs; 3584 scans were acquired for each spectrum with a recycle delay of 0.5 s. The transmission frequency (SFO1) is placed at 600 ppm. Spectra were analyzed by using Topspin version 3.5, Matlab version R2014b, and the Dmfit software.[52]

X-ray Diffraction. The structures and phase purity of Li_2MnO_3, LNMO, and LNMCO samples were determined by X-ray diffraction (XRD) using an X'PERT Pro MPD diffractometer (PANalytical) at 45 kV and 40 mA (Cu Kα radiation; λ = 0.15406 nm). The diffraction patterns were recorded in the 2θ range from 10° to 80°, with a scan rate of 7°/min.

RESULTS AND DISCUSSION

High-Resolution ^{7}Li pjMATPASS NMR for Site Quantification. Because of strong hyperfine interactions between unpaired electrons on TMs and Li spins, ^{7}Li NMR spectra of LMO cathodes show very broad signals with shift anisotropies

DOI: 10.1021/acs.chemmater.7b02589
Chem. Mater. 2017, 29, 8282−8291

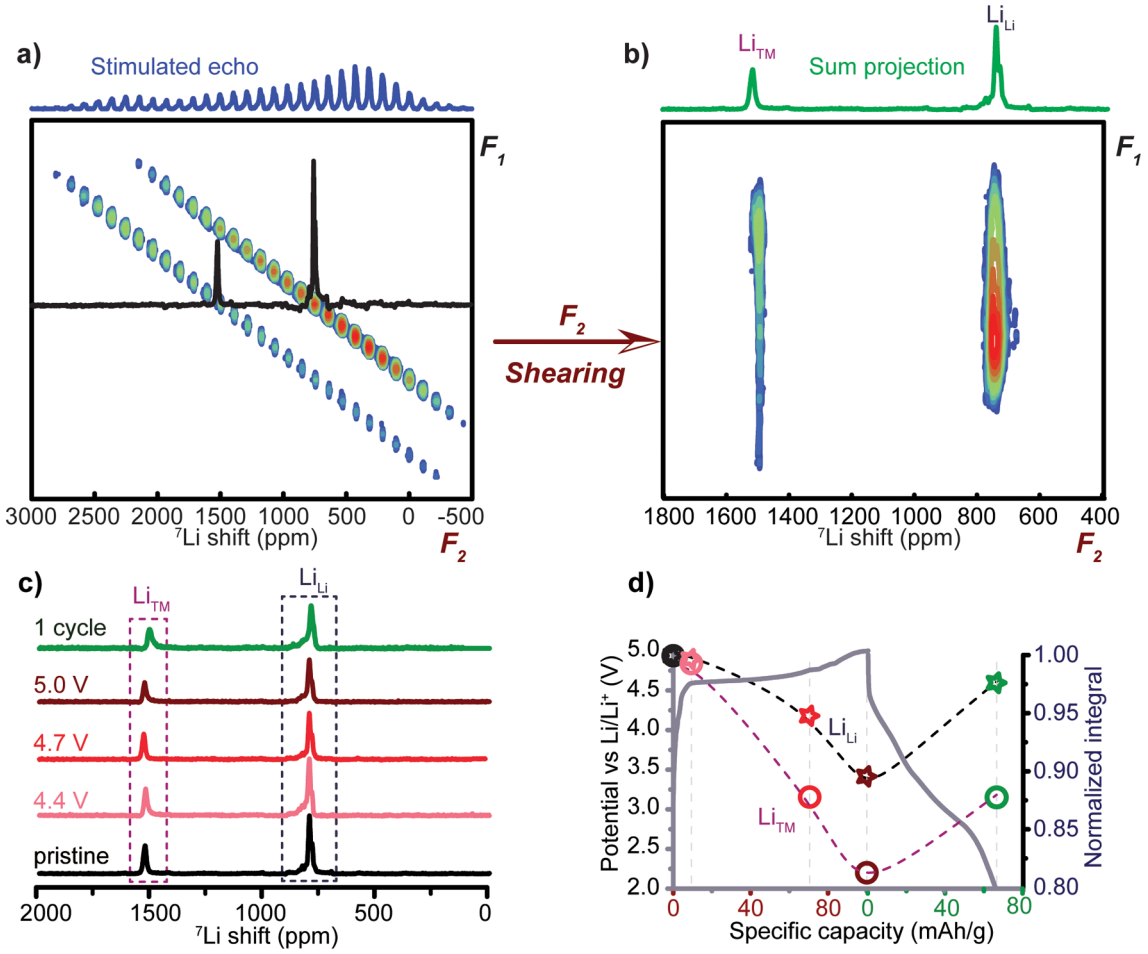

Figure 1. (a and b) pjMATPASS NMR of Li_2MnO_3 to achieve a pure isotropic spectrum. After spectral shearing has been performed along the F_2 dimension, (panel b) the row projection sum shows a pure isotropic ^7Li spectrum with two major resonances, which are assigned to Li_{TM} (with a Fermi contact shift of 1510 ppm) and Li_{Li} (750 ppm). As a comparison, a regular MAS spectrum obtained with a stimulated echo pulse sequence is shown on top of the pjMATPASS spectrum in panel a. (c) ^7Li isotropic NMR spectra of Li_2MnO_3 electrodes at different states of charge. (d) Normalized quantification of Li_{Li} and Li_{TM} in Li_2MnO_3 electrodes at different states of first charge and discharge. Spectra are calibrated on the basis of the sample mass and number of NMR acquisitions. The electrochemical profile of a Li_2MnO_3/Li half-cell battery is also shown.

of hundreds of kilohertz. In MAS ^7Li NMR, the large anisotropy manifests as manifolds of spinning sidebands, which are often overlapped with the main resonances of different Li local environments. An example is shown on top of the two-dimensional spectra in Figure 1a, the ^7Li spectrum of Li_2MnO_3 at a MAS rate of 50 kHz. The severe peak overlap prevents possible identification of different Li sites in Li_2MnO_3, not to mention quantification. To achieve the necessary high resolution for unambiguous site identification and reliable quantification, pjMATPASS[50] is employed to separate different orders of SSBs. Panels a and b of Figure 1 demonstrate the process for obtaining ^7Li NMR with pure isotropic peaks. The pjMATPASS experiment generates a pseudo-two-dimensional spectrum shown in Figure 1a, in which different orders of SSBs are distributed in sequential rows. The zeroth-order SSB containing only the isotropic peaks appears in the middle row, which shows two resonances at 750 and 1510 ppm from Li_{Li} and Li_{TM}, respectively. The peaks in the rest of the rows in the pseudo-two-dimensional are copies of these two resonances. The relative intensities of SSBs encode the parameters of shift anisotropy, which is characteristic of the local structures and compositions surrounding the Li sites of interest. The SSBs can be aligned vertically by spectral shearing (Figure 1b), and the projection of the sheared two-dimensional (2D) spectrum is composed of only pure isotropic peaks, similar to the central row. Each isotropic peak represents a unique Li local environment. Li_{Li} resonates at 750 ppm and Li_{TM} at 1510 ppm. Li_{TM} has a Fermi contact interaction with unpaired electrons on Mn^{4+} that is stronger than that for Li_{Li} because of different degrees of spin density transfer from Mn to Li; therefore, Li_{TM} exhibits a relatively larger Fermi contact shift. With these two Li sites well resolved, it is possible to perform accurate quantification of the lithiation and delithiation in paramagnetic Li-rich cathodes.

In the pristine Li_2MnO_3 cathodes, ~76% Li are found in Li layers and 24% Li in the TM layers. To follow the extraction and insertion of Li_{Li} and Li_{TM} in Li_2MnO_3 cathodes upon cycling, ^7Li pjMATPASS NMR is performed on Li_2MnO_3 cathodes charged to 4.4, 4.7, and 5.0 V and one discharged to 2.0 V: 4.4 V corresponds to the point of complete oxidation of residual Mn^{3+} to Mn^{4+}, 4.7 V is near the end of the O_2 evolution plateau, and 5.0 V is at the top of charge. One Li_2MnO_3 cathode at the end of the first discharge is also examined to evaluate the insertion of Li into Li_{Li} and Li_{TM} sites. The corresponding ^7Li spectra of Li_2MnO_3 cathodes at these states of charge are plotted in Figure 1c. Upon charge, the

DOI: 10.1021/acs.chemmater.7b02589
Chem. Mater. 2017, 29, 8282−8291

intensity of both Li_{Li} and Li_{TM} resonances gradually decreases, indicating that Li ions are extracted from both Li layers and TM layers. The total NMR signal of the Li_2MnO_3 cathode charged to 5.0 V is decreased by ~20% compared to that of pristine Li_2MnO_3, corresponding to 0.4 Li removed from Li_2MnO_3 and a charge capacity of 100.6 mAh/g. Li is reintercalated into the Li_xMnO_3 cathode upon discharge, and a higher-intensity ^7Li NMR signal is observed. It is worth noting that some minor and broad resonances emerge at the left foot of the 750 ppm peak, likely from Li at tetrahedral sites. It has been shown both experimentally and computationally that migration of Li from octahedral to tetrahedral sites is possible and this migration will lead to formation of spinel-like structural domains.[12,15,16]

Detailed quantification is performed on the basis of the area integral of Li_{Li} and Li_{TM} resonances at different states of charge, and the normalized quantification results are presented in Figure 1d. It shows that upon first charge, Li extraction slightly prefers Li_{TM}, with 20% Li_{TM} and 10% Li_{Li} removed. Upon discharge, ~87% Li_{TM} and 97% Li_{Li} are recovered compared to pristine Li_2MnO_3, implying that Li reintercalation preferentially takes place in the Li layer. These observations are consistent with the delithiation sequence proposed by previous computational works.[15,16] In addition, the spontaneous migration of Li from TM layers to vacated Li layers revealed by Persson and co-workers[15,16] explains the preference for extraction of Li from TM layers and reintercalation of Li into Li layers.

When Ni, in addition to Mn, is incorporated into the TM layers, to form LNMO compositions, the ^7Li spectra (Figure 2a) become more complex than those of Li_2MnO_3: (1) two shoulders are observed for Li in Li layers and TM layers; (2) Li_{TM} shows a relatively high field shift to 1500 ppm compared to that of pure Li_2MnO_3 at 1510 ppm; (3) much broader NMR peaks ranging from 300 to 1200 ppm are found for Li in the Li layer. The variation in shifts is due to the difference in spin density transfer between Ni and Mn to Li. The large peak width of the resonances originates from the heterogeneity of Ni and Mn coordination to Li.[18,49,53] At least three ^7Li local environments are found for both Li_{TM} and Li_{Li} via detailed analysis of the ^7Li pjMATPASS spectrum of pristine LNMO (Figure S3). High-resolution ^7Li NMR spectra are recorded on cycled LNMO cathodes to probe structural modification upon delithiation and lithiation: 4.4 V corresponds to complete oxidation of Ni^{2+} to Ni^{4+} and oxidation of residual Mn^{3+} to Mn^{4+}; 4.6 V is near the end of the O_2 evolution process; and 4.8 V is at the top of charge. One sample at the end of discharge is studied to probe lithiation reversibility. The intensity of Li_{TM} and Li_{Li} gradually decreases as Li ions are extracted from LNMO upon charge. When the charge reaches 4.8 V, the Li_{TM} peak disappears completely, while a small amount of Li_{Li} remains. Both Li_{TM} and Li_{Li} resonances return upon discharge. The two resonance peaks are significantly broadened due to rearrangement of local structures caused by Li extraction and intercalation. The intensity of one sharp peak located at 0 ppm increases through the whole electrochemical cycling process, which is attributed to solid−electrolyte interphase (SEI). This is not observed for the Li_2MnO_3 cathode (Figure 1c). The presence of Ni increases the specific capacity and meanwhile promotes SEI formation on the LNMO cathode.[54]

Results from quantitative analysis of the spectra in Figure 2a are shown in Figure 2b. Both Li_{TM} and Li_{Li} exhibit almost linear decay upon charge. The slope of the Li_{TM} decrease is slightly steeper than that for Li_{Li} at the beginning of the first charge, and Li_{TM} extraction slows at later stages of charge. At the top of the charge range (4.8 V), Li_{TM} is depleted and 20% Li_{Li} remains. The quantification results obtained with NMR are in good agreement with the remaining total Li content calculated from electrochemistry; 60% Li_{TM} and 90% Li_{Li} are reintercalated at the end of the first discharge. This again confirms that Li preferentially reintercalates into Li layers.[49,55]

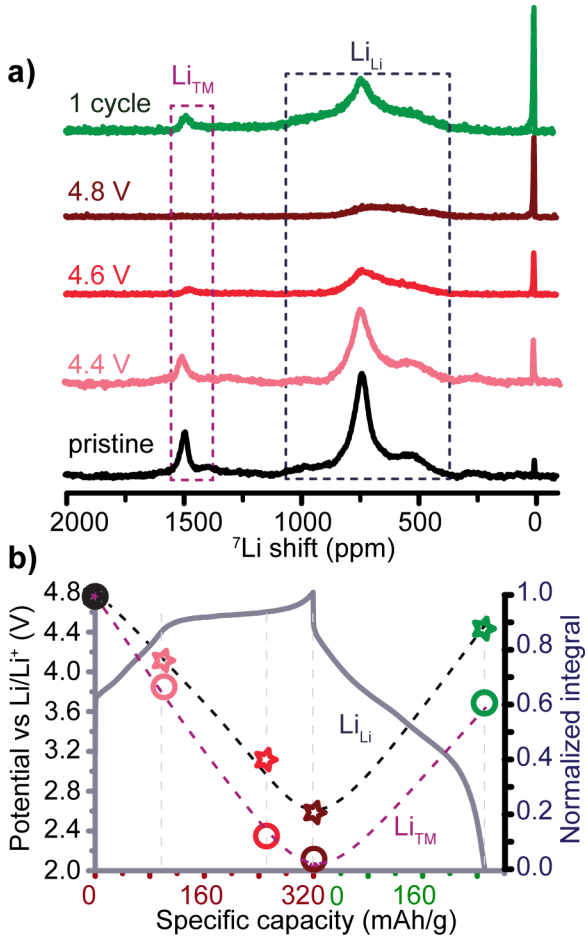

Figure 2. (a) ^7Li pjMATPASS NMR spectra of LNMO electrodes at different states of charge. (b) Electrochemical profile of a LNMO/Li half-cell battery and quantified evolution of Li_{TM} and Li_{Li} in LNMO electrodes during the first charge and discharge process.

Incorporating Co brings increased complexity to Li local structures in LNMCO compared to LNMO. Pristine LNMCO shows two groups of Li resonances as presented in Figure 3a. A cluster of peaks between 1200 and 1650 ppm is from Li in TM layers, and the other between 200 and 1000 ppm is from Li in Li layers. The Li_{TM} and Li_{Li} resonances can both be further decomposed into four major components via more detailed spectral analysis as shown in Figure S4. The different Li_{TM} peaks originate from variations in the neighboring coordination of Mn, Ni, and Co to Li, as shown in previous studies.[7,49,55] Li NMR spectra are recorded to probe the modification of LNMCO cathodes by (de)lithiation: 4.4 V corresponding to oxidation of Ni^{2+} to Ni^{4+}, Co^{3+} to Co^{4+}, and possibly residual Mn^{3+} to Mn^{4+}, 4.6 V next to the end of O_2 evolution, and 4.8 V at the top of the charge range. One sample at the end of the first discharge is studied to check (de)lithiation reversibility. It is found that Li ions are extracted from both Li layers and TM layers upon charge. At 4.8 V, Li_{TM} is depleted and residual Li_{Li} is observed. The spectrum of the cathode after one charge−discharge cycle shows both Li_{TM} and Li_{Li} resonances. However,

DOI: 10.1021/acs.chemmater.7b02589
Chem. Mater. 2017, 29, 8282−8291

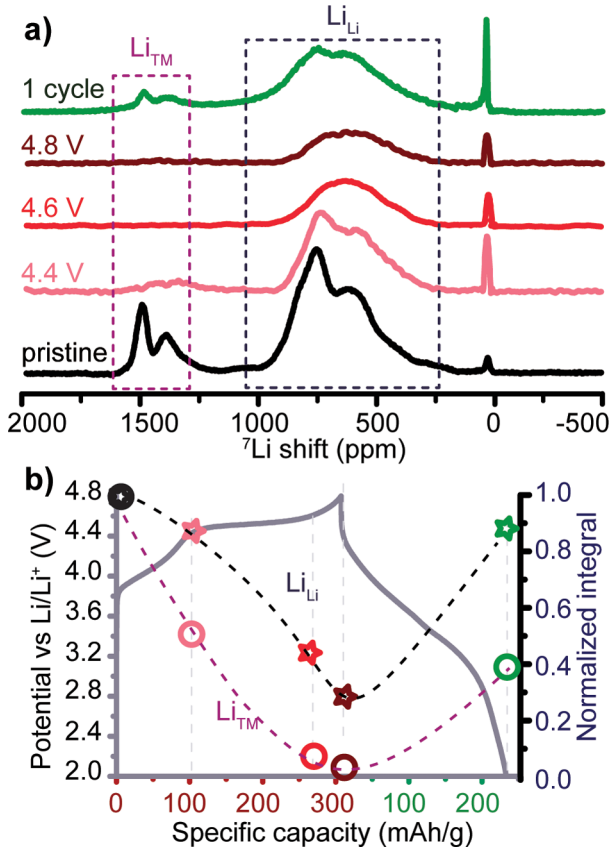

Figure 3. (a) ^{7}Li NMR spectra of LNMCO electrodes at different states of charge. (b) Electrochemical profile of a LNMCO/Li half-cell battery and quantified evolution of Li ions in Li layers and TM layers of LNMCO electrodes during the first charge and discharge process.

the two resonances are broadened, revealing structural disorder induced by the electrochemical cycling. Similar to LNMO, one sharp peak located at 0 ppm from SEI arises and grows rapidly upon cycling.

Quantification results of the lithiation and delithiation process within the LNMCO cathode are shown in Figure 3b. Both Li_{Li} and Li_{TM} show almost linear decay upon charge. At the beginning of charge, Li_{TM} shows a slope of decay steeper than that of Li_{Li}. At top of charge (4.8 V), there is no Li_{TM} left, while 30% Li_{Li} remains. Upon first discharge, approximately 40% (40% − 0%) and 60% (90% − 30%) of Li are reintercalated into TM and Li layers, respectively. This again suggests that Li preferentially reintercalates into Li layers.[49]

To compare the influence of different TMs on Li extraction and reinsertion, quantified and normalized delithiation and lithiation of the Li_2MnO_3, LNMO, and LNMCO cathodes are plotted in Figure 4. Capacities are normalized to the maximum experimental values of each cathode. The Coulombic efficiency is around 75% for LNMO and LNMCO and 62% for Li_2MnO_3 in the first cycle. Li_{TM} extraction is slightly preferred over Li_{Li} extraction at the beginning of the first charge in all three cathodes. The difference gap in Li_{Li} and Li_{TM} extraction is similar for Li_2MnO_3 and LNMO. However, Co in LNMCO seems to enhance this difference in the delithiation rate of Li_{TM} and Li_{Li}. Li quantification of the first discharge reveals a significant loss of Li_{TM} in all three Li-rich cathodes compared to their pristine states.

***Operando* ^{7}Li NMR for Real Time Monitoring of Li_{Li} and Li_{TM} Extraction and Insertion.** *Ex situ* pjMATPASS

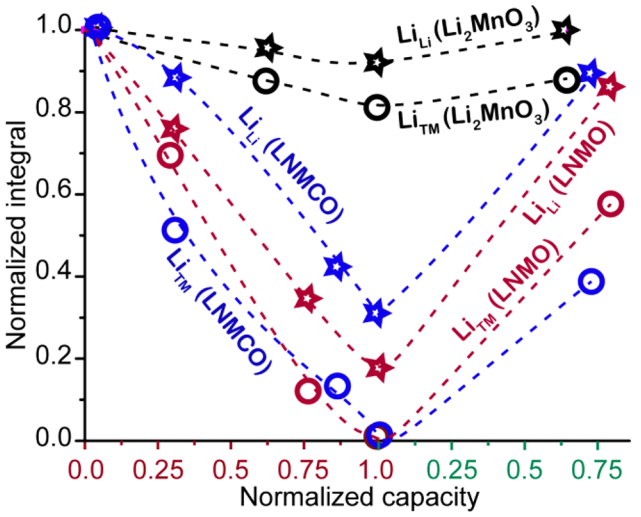

Figure 4. Comparison of ^{7}Li NMR signal integrals for cycled Li_2MnO_3, LNMO, and LNMCO electrodes. The data are adapted from Figures 1d, 2b, and 3b with axis values normalized to the respective experimental maximum capacity. Stars denote values for Li_{Li} and circles denotefor Li_{TM}.

NMR spectra provide clear assignments for different Li local environments and reliable quantification of different Li participation in the (de)lithiation process. Adding temporal resolution is helpful for examining Li extraction and insertion dynamics at different states of charge with finer steps. *Operando* NMR can follow Li evolution during battery cycling to offer insights that cannot be obtained from *ex situ* studies, especially real time Li extraction and reinsertion dynamics. Even though the resolution of static *operando* NMR is poor for the paramagnetic LMO cathode systems, it is sufficient to resolve Li_{Li} and Li_{TM}, making it possible to follow their individual evolution in real time.

Figure 5a shows the static ^{7}Li NMR spectrum of a pristine Li_2MnO_3//Li half-cell battery. The intense sharp peak at 250 ppm originates from the Li metal anode. The ^{7}Li NMR resonances of the Li_2MnO_3 cathode cover a broad range from −1000 to 2000 ppm. The major peak centered around 500 ppm is from Li_{Li} and the other one at ∼1400 ppm from Li_{TM}. The difference in peak positions in static and MAS NMR spectra is due to shift anisotropy and asymmetry parameters. The center of a static spectrum more often does not coincide with the isotropic peak position. Nevertheless, they represent the same Li local environment. Besides the broad resonances, a small sharp peak at 0 ppm is from Li salt in electrolyte LP30. Because the electrolyte is not of interest in this study, the experimental condition is optimized to achieve high temporal resolution while allowing full relaxation of Li resonances in LMO cathodes. As a result, the optimal recycle delay of 0.05 s between each NMR spectrum acquisition was used for both LMO cathodes and Li anodes.

Selective *operando* ^{7}Li NMR spectra are shown in Figure 5b for the first charge−discharge process. The three spectra plotted in thick black, red, and green lines correspond to the pristine cell, top of charge, and end of first discharge, respectively. The intensities of the broad signals from the Li_2MnO_3 cathode decrease upon charge due to Li extraction. Meanwhile, the intensity of the sharp peak at 250 ppm increases due to the deposition of Li onto a Li metal surface. The broad signal partially recovers upon discharge as Li is

DOI: 10.1021/acs.chemmater.7b02589
Chem. Mater. 2017, 29, 8282−8291

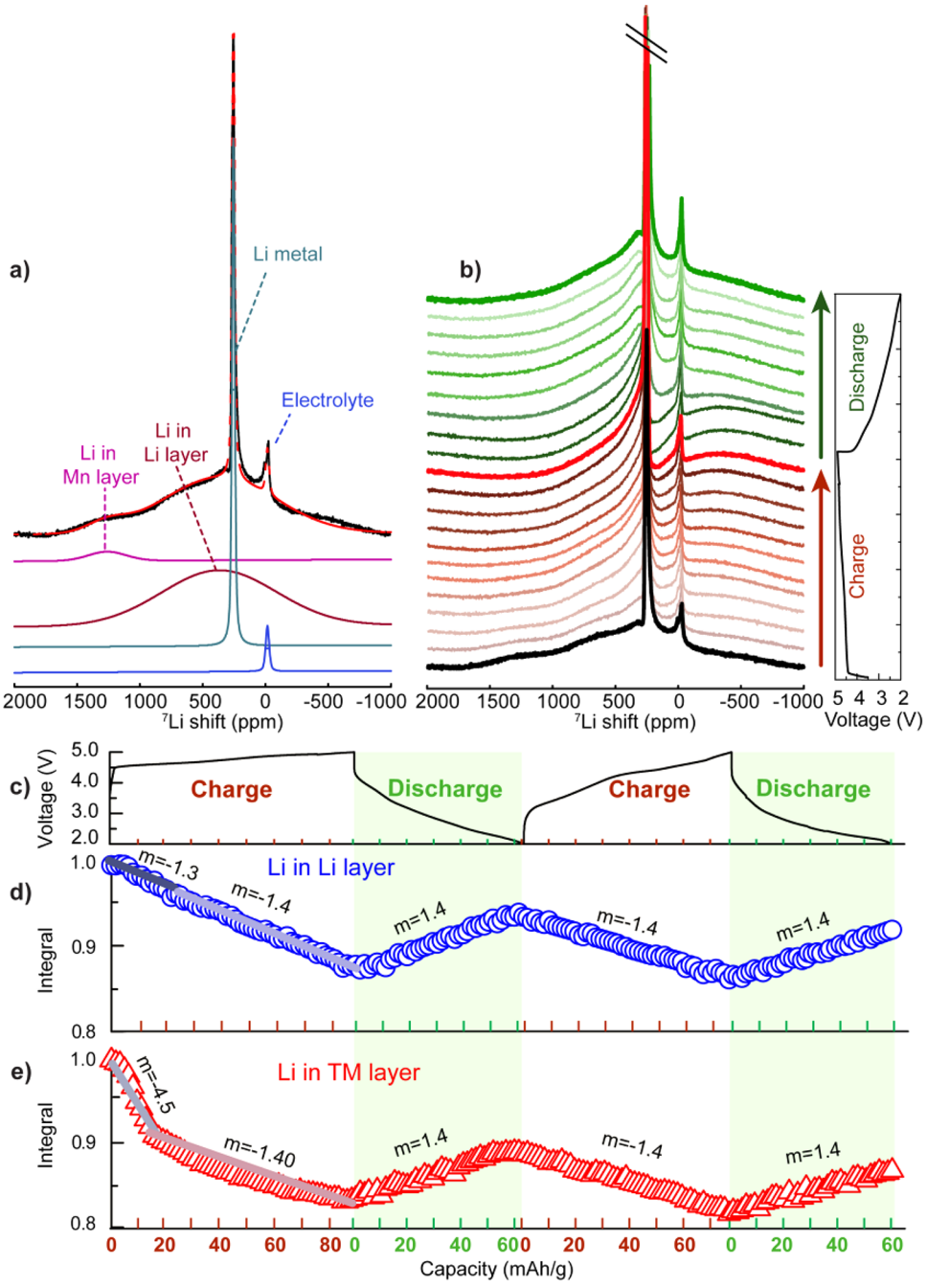

Figure 5. (a) ^{7}Li static NMR spectra of a pristine Li_2MnO_3//Li half-cell battery. The black spectrum was experimentally recorded, and the red-dash line is the sum of simulated individual ^{7}Li components from the electrolyte, Li metal anode, and Li_2MnO_3 cathode. (b) Selective *operando* ^{7}Li NMR spectra during the first charge−discharge cycle with the corresponding electrochemical profile. (c) Electrochemical profile of a Li_2MnO_3//Li half-cell battery in the working voltage range between 2.0 and 5.0 V. (d and e) Normalized area integrals of NMR resonances of Li in Li layers and TM layers, respectively, in *operando* ^{7}Li NMR spectra.

reintercalated into the Li_2MnO_3 cathode. On the other hand, the intensity of the Li anode NMR signal decreases due to Li stripping upon discharge. It is worth noting that upon charge, the phase of the Li metal peak is significantly distorted because of the magnetic susceptibility effects on the newly formed Li microstructure (moss and dendrite).[56] The phase returns to normal upon discharge as the Li microstructure on the anode is removed.

The electrochemical profile of the first two charge−discharge cycles for a Li_2MnO_3//Li half-cell battery is shown in Figure 5c. Specific capacities of 90 and ∼80 mAh/g are obtained for the first and second charges, respectively, a specific capacity of ∼60 mAh/g was obtained for both first and second discharge. It is worth pointing out that Li_2MnO_3 does not make a high-capacity cathode for rechargeable batteries; nevertheless, it is a clean and representative system for studying Li extraction dynamics in Li-rich cathodes. Quantification of Li in both the Li layer and the TM layer, based on area integrals of corresponding NMR resonances in *operando* ^{7}Li NMR spectra (Figure 5a), is performed (panels d and e of Figure 5, respectively). The extraction of Li_{Li} from Li_2MnO_3 is relatively slow at the beginning of first charge (dark blue region) with a

DOI: 10.1021/acs.chemmater.7b02589
Chem. Mater. 2017, 29, 8282−8291

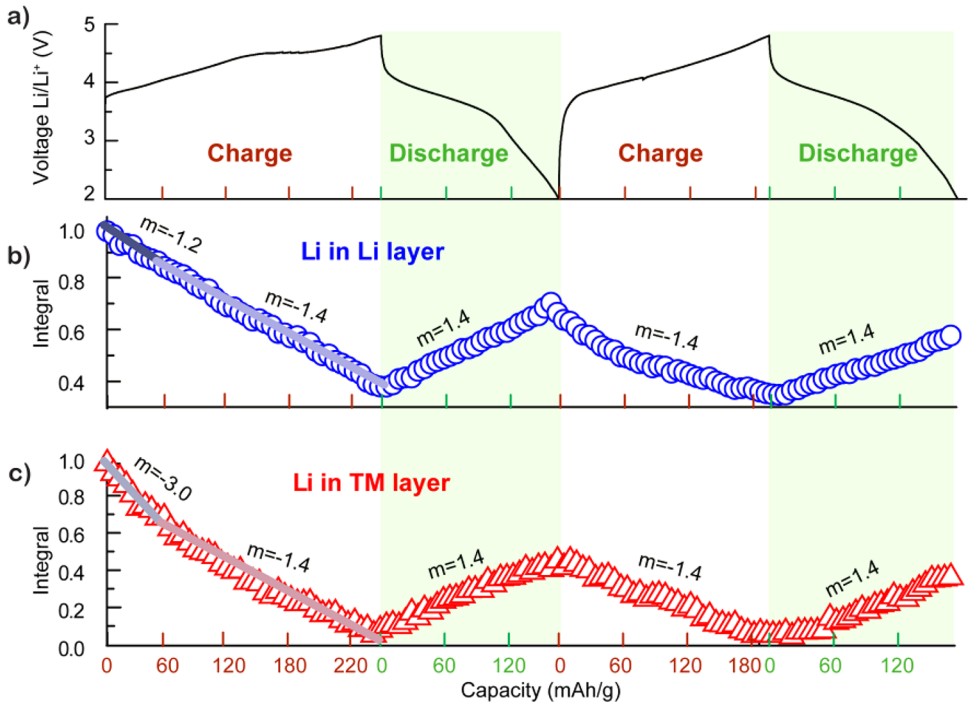

Figure 6. (a) Electrochemical profile of a LNMO//Li half-cell battery in the working voltage range of 2.0 and 4.8 V. (b and c) Normalized area integrals of NMR resonances from Li in Li layers and TM layers, respectively, vs specific capacity. The corresponding *operando* ^{7}Li NMR spectra are shown in Figure S6.

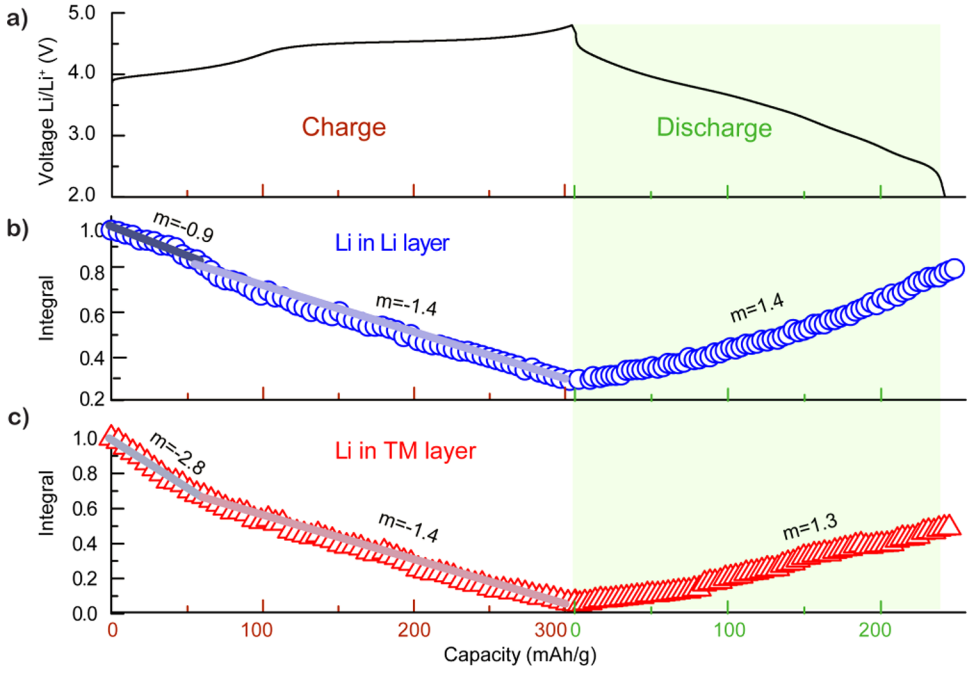

Figure 7. (a) Electrochemical profile of a LNMCO//Li half-cell battery in the working voltage range between 2.0 and 4.8 V. (b and c) Normalized area integrals of Li_{Li} and Li_{TM} resonances, respectively. The corresponding *operando* ^{7}Li NMR spectra are shown in Figure S7.

slope of $m = -1.3$ in the normalized NMR integral versus capacity plot (Figure 5d). Afterward, a slightly faster extraction is observed with $m = -1.4$. For Li_{TM}, it shows fast extraction at the very beginning of charge ($m = -4.5$) and slow removal at the later stage of charge ($m = -1.4$). Li_{Li} and Li_{TM} show similar rates of insertion and extraction after the first charge. The activation of Li_2MnO_3 starts with extraction of Li_{TM}. Li_{Li} and Li_{TM} both show lower-intensity NMR signals after the first and second cycle compared with their corresponding amounts in pristine Li_2MnO_3, which reflects the fact that the process of Li extraction and reinsertion is not completely reversible, consistent with electrochemistry. Also, the quantified *operando* experimental data help us to understand the contribution of each Li structural site to the specific capacity at various states of charge.

DOI: 10.1021/acs.chemmater.7b02589
Chem. Mater. 2017, 29, 8282−8291

The Li_2MnO_3 cathode is a relatively simple and clean model compound for determining the Li extraction and insertion dynamics. In the following, we extend our investigations to more complex and practical Li-rich cathodes: LNMO and LNMCO. When other TMs in addition to Mn are incorporated into the LMO structure, more Li ions can be extracted because of the increased amount of TMs with redox-active pairs per unit mass,[14] and the additional TMs can stabilize the structure and allow more Li extraction to take place.[9] With *operando* NMR, the Li extraction and insertion dynamics for Li in both Li layers and TM layers in LNMO and LNMCO are determined.

For the LNMO cathode, a specific capacity of 240 mAh/g is achieved for the first charge as shown in Figure 6a. Assuming all Ni^{2+} is oxidized to Ni^{4+}, it offers a capacity of ∼120 mAh/g. The extra capacity of C = 120 mAh/g has to originate from the oxidation of O^{2-} mainly over the plateau at 4.5 V. The first discharge achieves a capacity of 170 mAh/g, originating from the reduction of Ni^{4+}, Mn^{4+}, and possibly $(O)_2^{n-}$.[9,57] The second charge delivers a capacity of C = 190 mAh/g and second discharge a capacity of C = 170 mAh/g.

Operando ^{7}Li NMR quantifications of the LNMO cathode in a LNMO//Li half-cell battery, based on spectra collected in real time with battery cycling (Figure S7), are shown in panels b and c of Figure 6. A slower decay (m = −1.2) and a faster decay (m = −3.0) are observed for Li_{Li} and Li_{TM}, respectively, at the beginning of the first charge. This behavior reflects the fact that the activating process starts from the TM layer for the LNMO cathode. After the activating process, the Li extraction and reinsertion for Li in both Li layers and TM layers behave linearly (Figure 6b,c), with a similar (de)lithiation rate of m = −1.4. At top of charge, Li in TM layer is completely removed (Figure 6c); however, there is still ∼40% residual Li in the Li layer. Upon the first discharge, Li_{Li} is restored to 70% and Li_{TM} to 40% compared with their respective amounts in pristine LNMO. No preferential extraction or insertion of Li_{Li} and Li_{TM} is observed for the second charge and discharge cycle, suggested by the same slope of $|m|$ = 1.4.

When Co is introduced into the TM layer in addition to Mn and Ni to form another Li-rich cathode, LNMCO, a capacity of 305 mAh/g is obtained for the first charge (Figure 7a). Below 4.5 V during charge, oxidation of Ni^{2+} and Co^{3+} occurs to produce a capacity of ∼120 mAh/g. The long plateau around 4.5 V is mainly associated with O^{2-} oxidation, yielding a capacity of 160 mAh/g. The first discharge provides a capacity of C = 240 mAh/g, which is attributed to the reduction of Ni^{4+}, Co^{4+}, Mn^{4+}, and possibly O_2^{n-}.

Quantified analysis of the *operando* ^{7}Li NMR on the LNMCO cathode (Figure S7) is presented in panels b and c of Figure 7. As in Li_2MnO_3 and LNMO, a slower linear decay with a slope of m = −0.9 for Li_{Li} and a faster linear decay with a slope of m = −2.8 for Li_{TM} are observed at the very beginning of the first charge. This behavior implies that initial charge largely prefers to extract Li from the TM layers for the LNMCO cathode. At the later stage of charge and the following discharge, no preference is observed for Li_{Li} or Li_{TM}. The Li extraction and insertion show the same rate for both Li_{Li} and Li_{TM} with a slope of $|m|$ = 1.4. At the top of charge, Li_{TM} is completely removed (Figure 7c), but ∼30% Li_{Li} remains. Incomplete reinsertion is observed on the basis of the lower intensity of the NMR signal for both Li_{Li} (83%) and Li_{TM} (45%) in LNMCO.

By comparison of Li_{Li} and Li_{TM} extraction and insertion dynamics within $LiMn_2O_3$, LNMO, and LNMCO cathodes obtained from NMR, it reveals that Li is preferentially extracted from TM layers at the beginning of charge, approximately up to 20% of the practical first charge capacity, in all three cathodes. This initial selective removal of Li from TM layers occurs only once and seems to serve as a conditioning step of the Li-rich cathodes. Uniform Li extraction and insertion of Li_{Li} and Li_{TM} are observed afterward and in the following charge−discharge cycles. Significant irreversible loss of Li in TM layers is seen in all three cathodes, 12% for $LiMn_2O_3$, 40% for LNMO, and 60% for LNMCO, while irreversible loss of Li from Li layers is 7% for $LiMn_2O_3$, 10% for LNMO, and 10% for LNMCO. The presence of Ni and Co promotes full extraction of Li from TM layers at the end of charge, and the remaining Li, if any, all resides in the Li layer. It is worth noting that Ni and Co also seem to induce much more SEI formation on the cathodes compared with Ni- and Co-free Li_2MnO_3 does. When the Li extraction and insertion are coupled with electrochemistry, it shows that the irreversible capacity is mainly from the permanent loss of Li in TM layers.

CONCLUSIONS

This study combines two techniques for achieving high spectral and temporal resolution for quantitative real time monitoring of Li extraction and insertion dynamics in typical Li-rich cathodes. ^{7}Li pjMATPASS NMR is employed to obtain the highest spectral resolution to clearly distinguish and quantify various Li local environments. Optimized *operando* NMR is implemented for high temporal resolution to monitor lithiation and delithiation dynamics of various Li sites in real time. Both *ex situ* ^{7}Li pjMATPASS and *operando* NMR investigations consistently show that Li extraction starts preferably from TM layers, and this preference lasts until approximately 20% of the practical capacity is reached. After this initial conditioning, a similar rate of extraction of Li from and reinsertion of Li into both TM and Li layers is observed in Li_2MnO_3, LNMO, and LNMCO. Significant residual Li in both TM and Li layers is seen in Li_2MnO_3 cathodes. Complete extraction of Li from TM layers is achieved in LNMO and LNMCO, but the recovery of Li in TM layers upon discharge is <50% in LNMO and LNMCO cathodes, comparatively much lower than that of Li in Li layers. The combination of pjMATPASS with high spectral resolution and *operando* NMR with high temporal resolution provides a reliable quantitative approach to probing (de)-lithiation dynamics of different Li sites in paramagnetic cathodes. This method can be easily extended to other paramagnetic materials with large NMR shift anisotropies, such as Cu-, Fe-, and Mn-based Li and Na cathodes.

ASSOCIATED CONTENT

Supporting Information

The Supporting Information is available free of charge on the ACS Publications website at DOI: 10.1021/acs.chemmater.7b02589.

XRD patterns and NMR spectral simulations together with quantification of Li anodes upon cycling (PDF)

AUTHOR INFORMATION

Corresponding Author

*E-mail: hu@chem.fsu.edu.

ORCID

Mingxue Tang: 0000-0002-7282-4100

DOI: 10.1021/acs.chemmater.7b02589
Chem. Mater. 2017, 29, 8282−8291

Author Contributions

X.L. and M.T. contributed equally to this work, and the names are listed in alphabetical order.

Notes

The authors declare no competing financial interest.

■ ACKNOWLEDGMENTS

This work was supported the National Science Foundation under Grant DMR-1508404. All the NMR experiments were performed at the National High Magnetic Field Laboratory, which is funded by the NSF under contract DMR-1157490.

■ ABBREVIATIONS

NMR, nuclear magnetic resonance; MAS, magic-angle spinning; pjMATPASS, projection magic-angle turning and phase-adjusted sideband separation; XRD, X-ray diffraction; SSBs, spinning sidebands; LNMO, $Li_{1.2}Ni_{0.2}Mn_{0.6}O_2$; LNMCO, $Li_{1.2}Ni_{0.13}Mn_{0.54}Co_{0.13}O_2$

■ REFERENCES

(1) Tarascon, J.-M.; Armand, M. Issues and Challenges Facing Rechargeable Lithium Batteries. *Nature* **2001**, *414* (6861), 359−367.

(2) Armand, M.; Tarascon, J.-M. Building Better Batteries. *Nature* **2008**, *451* (7179), 652−657.

(3) Chen, Z.; Ren, Y.; Lee, E.; Johnson, C.; Qin, Y.; Amine, K. Study of Thermal Decomposition of Li1-x(Ni1/3Mn1/3Co1/3)0.9O2 Using In-Situ High-Energy X-Ray Diffraction. *Adv. Energy Mater.* **2013**, *3* (6), 729−736.

(4) Chen, R.; Ren, S.; Knapp, M.; Wang, D.; Witter, R.; Fichtner, M.; Hahn, H. Disordered Lithium-Rich Oxyfluoride as a Stable Host for Enhanced Li+ Intercalation Storage. *Adv. Energy Mater.* **2015**, *5* (9), 1401814−1401820.

(5) Manthiram, A.; Knight, J. C.; Myung, S.-T.; Oh, S.-M.; Sun, Y.-K. Nickel-Rich and Lithium-Rich Layered Oxide Cathodes: Progress and Perspectives. *Adv. Energy Mater.* **2016**, *6* (1), 1501010−1501032.

(6) He, M.; Su, C.-C.; Feng, Z.; Zeng, L.; Wu, T.; Bedzyk, M. J.; Fenter, P.; Wang, Y.; Zhang, Z. High Voltage LiNi0.5Mn0.3Co0.2O2/Graphite Cell Cycled at 4.6 V with a FEC/HFDEC-Based Electrolyte. *Adv. Energy Mater.* **2017**, *7*, 1700109−1700117.

(7) Luo, K.; Roberts, M. R.; Hao, R.; Guerrini, N.; Pickup, D. M.; Liu, Y.-S.; Edström, K.; Guo, J.; Chadwick, A. V.; Duda, L. C.; Bruce, P. G. Charge-Compensation in 3d-Transition-Metal-Oxide Intercalation Cathodes through the Generation of Localized Electron Holes on Oxygen. *Nat. Chem.* **2016**, *8* (7), 684−691.

(8) Seo, D.-H.; Lee, J.; Urban, A.; Malik, R.; Kang, S.; Ceder, G. The Structural and Chemical Origin of the Oxygen Redox Activity in Layered and Cation-Disordered Li-Excess Cathode Materials. *Nat. Chem.* **2016**, *8* (7), 692−697.

(9) Rozier, P.; Tarascon, J. M. Review—Li-Rich Layered Oxide Cathodes for Next-Generation Li-Ion Batteries: Chances and Challenges. *J. Electrochem. Soc.* **2015**, *162* (14), A2490−A2499.

(10) Kim, J.-S.; Johnson, C. S.; Vaughey, J. T.; Thackeray, M. M.; Hackney, S. A.; Yoon, W.; Grey, C. P. Electrochemical and Structural Properties of XLi2M'O3·(1−x)LiMn0.5Ni0.5O2 Electrodes for Lithium Batteries (M' = Ti, Mn, Zr; $0 \leq x \leqslant 0.3$). *Chem. Mater.* **2004**, *16* (10), 1996−2006.

(11) Meng, Y. S.; Ceder, G.; Grey, C. P.; Yoon, W.-S.; Jiang, M.; Bréger, J.; Shao-Horn, Y. Cation Ordering in Layered O3 Li[NixLi1/3−2x/3Mn2/3-x/3]O2 ($0 \leq x \leq 1/2$) Compounds. *Chem. Mater.* **2005**, *17* (9), 2386−2394.

(12) Van der Ven, A.; Ceder, G. Ordering in Lix(Ni0.5Mn0.5)O2 and Its Relation to Charge Capacity and Electrochemical Behavior in Rechargeable Lithium Batteries. *Electrochem. Commun.* **2004**, *6* (10), 1045−1050.

(13) Bréger, J.; Meng, Y. S.; Hinuma, Y.; Kumar, S.; Kang, K.; Shao-Horn, Y.; Ceder, G.; Grey, C. P. Effect of High Voltage on the Structure and Electrochemistry of LiNi0.5Mn0.5O2: A Joint Experimental and Theoretical Study. *Chem. Mater.* **2006**, *18* (20), 4768−4781.

(14) Kang, K.; Meng, Y. S.; Bréger, J.; Grey, C. P.; Ceder, G. Electrodes with High Power and High Capacity for Rechargeable Lithium Batteries. *Science* **2006**, *311* (5763), 977−980.

(15) Lee, E.; Persson, K. A. Structural and Chemical Evolution of the Layered Li-Excess $Li_x MnO_3$ as a Function of Li Content from First-Principles Calculations. *Adv. Energy Mater.* **2014**, *4* (15), 1400498.

(16) Shin, Y.; Ding, H.; Persson, K. A. Revealing the Intrinsic Li Mobility in the $Li_2 MnO_3$ Lithium-Excess Material. *Chem. Mater.* **2016**, *28* (7), 2081−2088.

(17) Liu, H.; Chen, Y.; Hy, S.; An, K.; Venkatachalam, S.; Qian, D.; Zhang, M.; Meng, Y. S. Operando Lithium Dynamics in the Li-Rich Layered Oxide Cathode Material via Neutron Diffraction. *Adv. Energy Mater.* **2016**, *6* (7), 1502143−1502149.

(18) Grey, C. P.; Dupré, N. NMR Studies of Cathode Materials for Lithium-Ion Rechargeable Batteries. *Chem. Rev.* **2004**, *104* (10), 4493−4512.

(19) Chernova, N. A.; Ma, M.; Xiao, J.; Whittingham, M. S.; Breger, J.; Grey, C. P. Layered LixNiyMnyCo1−2yO2 Cathodes for Lithium Ion Batteries: Understanding Local Structure via Magnetic Properties. *Chem. Mater.* **2007**, *19* (19), 4682−4693.

(20) Jiang, M.; Key, B.; Meng, Y. S.; Grey, C. P. Electrochemical and Structural Study of the Layered, "Li-Excess" Lithium-Ion Battery Electrode Material Li[Li1/9Ni1/3Mn5/9]O2. *Chem. Mater.* **2009**, *21* (13), 2733−2745.

(21) Zeng, D.; Cabana, J.; Yoon, W.-S.; Grey, C. P. Investigation of the Structural Changes in Li[NiyMnyCo(1−2y)]O2 (y = 0.05) upon Electrochemical Lithium Deintercalation. *Chem. Mater.* **2010**, *22* (3), 1209−1219.

(22) Rosina, K. J.; Jiang, M.; Zeng, D.; Salager, E.; Best, A. S.; Grey, C. P. Structure of Aluminum Fluoride Coated Li[Li1/9Ni1/3Mn5/9]O2 Cathodes for Secondary Lithium-Ion Batteries. *J. Mater. Chem.* **2012**, *22* (38), 20602−20610.

(23) Hu, Y.-Y.; Liu, Z.; Nam, K.-W.; Borkiewicz, O. J.; Cheng, J.; Hua, X.; Dunstan, M. T.; Yu, X.; Wiaderek, K. M.; Du, L.-S.; Chapman, K. W.; Chupas, P. J.; Yang, X.-Q.; Grey, C. P. Origin of Additional Capacities in Metal Oxide Lithium-Ion Battery Electrodes. *Nat. Mater.* **2013**, *12* (12), 1130−1136.

(24) Seymour, I. D.; Middlemiss, D. S.; Halat, D. M.; Trease, N. M.; Pell, A. J.; Grey, C. P. Characterizing Oxygen Local Environments in Paramagnetic Battery Materials via 17O NMR and DFT Calculations. *J. Am. Chem. Soc.* **2016**, *138* (30), 9405−9408.

(25) Trease, N. M.; Seymour, I. D.; Radin, M. D.; Liu, H.; Liu, H.; Hy, S.; Chernova, N.; Parikh, P.; Devaraj, A.; Wiaderek, K. M.; Chupas, P. J.; Chapman, K. W.; Whittingham, M. S.; Meng, Y. S.; Van der Van, A.; Grey, C. P. Identifying the Distribution of Al3+ in LiNi0.8Co0.15Al0.05O2. *Chem. Mater.* **2016**, *28* (22), 8170−8180.

(26) Pecher, O.; Carretero-González, J.; Griffith, K. J.; Grey, C. P. Materials' Methods: NMR in Battery Research. *Chem. Mater.* **2017**, *29* (1), 213−242.

(27) Key, B.; Bhattacharyya, R.; Morcrette, M.; Seznéc, V.; Tarascon, J.-M.; Grey, C. P. Real-Time NMR Investigations of Structural Changes in Silicon Electrodes for Lithium-Ion Batteries. *J. Am. Chem. Soc.* **2009**, *131* (26), 9239−9249.

(28) Bhattacharyya, R.; Key, B.; Chen, H.; Best, A. S.; Hollenkamp, A. F.; Grey, C. P. Situ NMR Observation of the Formation of Metallic Lithium Microstructures in Lithium Batteries. *Nat. Mater.* **2010**, *9* (6), 504−510.

(29) Chandrashekar, S.; Trease, N. M.; Chang, H. J.; Du, L.-S.; Grey, C. P.; Jerschow, A. 7Li MRI of Li Batteries Reveals Location of Microstructural Lithium. *Nat. Mater.* **2012**, *11* (4), 311−315.

(30) Blanc, F.; Leskes, M.; Grey, C. P. Situ Solid-State NMR Spectroscopy of Electrochemical Cells: Batteries, Supercapacitors, and Fuel Cells. *Acc. Chem. Res.* **2013**, *46* (9), 1952−1963.

(31) Chang, H. J.; Ilott, A. J.; Trease, N. M.; Mohammadi, M.; Jerschow, A.; Grey, C. P. Correlating Microstructural Lithium Metal

DOI: 10.1021/acs.chemmater.7b02589
Chem. Mater. 2017, 29, 8282−8291

Growth with Electrolyte Salt Depletion in Lithium Batteries Using 7Li MRI. *J. Am. Chem. Soc.* **2015**, *137* (48), 15209−15216.
(32) Chang, H. J.; Trease, N. M.; Ilott, A. J.; Zeng, D.; Du, L.-S.; Jerschow, A.; Grey, C. P. Investigating Li Microstructure Formation on Li Anodes for Lithium Batteries by in Situ 6Li/7Li NMR and SEM. *J. Phys. Chem. C* **2015**, *119* (29), 16443−16451.
(33) Griffin, J. M.; Forse, A. C.; Tsai, W.-Y.; Taberna, P.-L.; Simon, P.; Grey, C. P. Situ NMR and Electrochemical Quartz Crystal Microbalance Techniques Reveal the Structure of the Electrical Double Layer in Supercapacitors. *Nat. Mater.* **2015**, *14* (8), 812−819.
(34) Zhou, L.; Leskes, M.; Liu, T.; Grey, C. P. Probing Dynamic Processes in Lithium-Ion Batteries by In Situ NMR Spectroscopy: Application to Li1.08Mn1.92O4 Electrodes. *Angew. Chem., Int. Ed.* **2015**, *54* (49), 14782−14786.
(35) Ilott, A. J.; Mohammadi, M.; Chang, H. J.; Grey, C. P.; Jerschow, A. Real-Time 3D Imaging of Microstructure Growth in Battery Cells Using Indirect MRI. *Proc. Natl. Acad. Sci. U. S. A.* **2016**, *113* (39), 10779−10784.
(36) Tang, M.; Sarou-Kanian, V.; Melin, P.; Leriche, J.-B.; Ménétrier, M.; Tarascon, J.-M.; Deschamps, M.; Salager, E. Following Lithiation Fronts in Paramagnetic Electrodes with in Situ Magnetic Resonance Spectroscopic Imaging. *Nat. Commun.* **2016**, *7*, 13284.
(37) Grey, C. P.; Tarascon, J. M. Sustainability and in Situ Monitoring in Battery Development. *Nat. Mater.* **2017**, *16* (1), 45−56.
(38) Lee, Y. J.; Wang, F.; Grey, C. P. 6Li and 7Li MAS NMR Studies of Lithium Manganate Cathode Materials. *J. Am. Chem. Soc.* **1998**, *120* (48), 12601−12613.
(39) Paik, Y.; Grey, C. P.; Johnson, C. S.; Kim, J.-S.; Thackeray, M. M. Lithium and Deuterium NMR Studies of Acid-Leached Layered Lithium Manganese Oxides. *Chem. Mater.* **2002**, *14* (12), 5109−5115.
(40) Pan, C.; Lee, Y. J.; Ammundsen, B.; Grey, C. P. 6Li MAS NMR Studies of the Local Structure and Electrochemical Properties of Cr-Doped Lithium Manganese and Lithium Cobalt Oxide Cathode Materials for Lithium-Ion Batteries. *Chem. Mater.* **2002**, *14* (5), 2289−2299.
(41) Carlier, D.; Ménétrier, M.; Grey, C. P.; Delmas, C.; Ceder, G. Understanding the NMR Shifts in Paramagnetic Transition Metal Oxides Using Density Functional Theory Calculations. *Phys. Rev. B: Condens. Matter Mater. Phys.* **2003**, *67* (17), 174103.
(42) Yoon, W.-S.; Kim, N.; Yang, X.-Q.; McBreen, J.; Grey, C. P. 6Li MAS NMR and in Situ X-Ray Studies of Lithium Nickel Manganese Oxides. *J. Power Sources* **2003**, *119*−*121*, 649−653.
(43) Armstrong, A. R.; Dupre, N.; Paterson, A. J.; Grey, C. P.; Bruce, P. G. Combined Neutron Diffraction, NMR, and Electrochemical Investigation of the Layered-to-Spinel Transformation in LiMnO2. *Chem. Mater.* **2004**, *16* (16), 3106−3118.
(44) Grey, C. P.; Yoon, W.-S.; Reed, J.; Ceder, G. Electrochemical Activity of Li in the Transition-Metal Sites of O3 Li [Li (1 − 2x)/3Mn (2 − x)/3Ni x] O 2. *Electrochem. Solid-State Lett.* **2004**, *7* (9), A290−A293.
(45) Bréger, J.; Dupré, N.; Chupas, P. J.; Lee, P. L.; Proffen, T.; Parise, J. B.; Grey, C. P. Short- and Long-Range Order in the Positive Electrode Material, Li(NiMn)0.5O2: A Joint X-Ray and Neutron Diffraction, Pair Distribution Function Analysis and NMR Study. *J. Am. Chem. Soc.* **2005**, *127* (20), 7529−7537.
(46) Bréger, J.; Jiang, M.; Dupré, N.; Meng, Y. S.; Shao-Horn, Y.; Ceder, G.; Grey, C. P. High-Resolution X-Ray Diffraction, DIFFaX, NMR and First Principles Study of Disorder in the Li2MnO3−Li[Ni1/2Mn1/2]O2 Solid Solution. *J. Solid State Chem.* **2005**, *178* (9), 2575−2585.
(47) Shimoda, K.; Murakami, M.; Komatsu, H.; Arai, H.; Uchimoto, Y.; Ogumi, Z. Delithiation/Lithiation Behavior of LiNi0.5Mn1.5O4 Studied by In Situ and Ex Situ 6,7Li NMR Spectroscopy. *J. Phys. Chem. C* **2015**, *119* (24), 13472−13480.
(48) Buzlukov, A.; Mouesca, J.-M.; Buannic, L.; Hediger, S.; Simonin, L.; Canevet, E.; Colin, J.-F.; Gutel, T.; Bardet, M. Li-Rich Mn/Ni Layered Oxide as Electrode Material for Lithium Batteries: A 7Li MAS NMR Study Revealing Segregation into (Nanoscale) Domains with Highly Different Electrochemical Behaviors. *J. Phys. Chem. C* **2016**, *120* (34), 19049−19063.
(49) Dogan, F.; Long, B. R.; Croy, J. R.; Gallagher, K. G.; Iddir, H.; Russell, J. T.; Balasubramanian, M.; Key, B. Re-Entrant Lithium Local Environments and Defect Driven Electrochemistry of Li- and Mn-Rich Li-Ion Battery Cathodes. *J. Am. Chem. Soc.* **2015**, *137* (6), 2328−2335.
(50) Hung, I.; Zhou, L.; Pourpoint, F.; Grey, C. P.; Gan, Z. Isotropic High Field NMR Spectra of Li-Ion Battery Materials with Anisotropy > 1 MHz. *J. Am. Chem. Soc.* **2012**, *134* (4), 1898−1901.
(51) Shunmugasundaram, R.; Senthil Arumugam, R.; Harris, K. J.; Goward, G. R.; Dahn, J. R. A Search for Low-Irreversible Capacity and High-Reversible Capacity Positive Electrode Materials in the Li−Ni−Mn−Co Pseudoquaternary System. *Chem. Mater.* **2016**, *28* (1), 55−66.
(52) Massiot, D.; Fayon, F.; Capron, M.; King, I.; Le Calvé, S.; Alonso, B.; Durand, J.-O.; Bujoli, B.; Gan, Z.; Hoatson, G. Modelling One- and Two-Dimensional Solid-State NMR Spectra. *Magn. Reson. Chem.* **2002**, *40* (1), 70−76.
(53) Yoon, W.-S.; Iannopollo, S.; Grey, C. P.; Carlier, D.; Gorman, J.; Reed, J.; Ceder, G. Local Structure and Cation Ordering in O3 Lithium Nickel Manganese Oxides with Stoichiometry Li [Ni x Mn (2 − x)/3Li (1 − 2x)/3] O 2 NMR Studies and First Principles Calculations. *Electrochem. Solid-State Lett.* **2004**, *7* (7), A167−A171.
(54) Oh, P.; Oh, S.-M.; Li, W.; Myeong, S.; Cho, J.; Manthiram, A. High-Performance Heterostructured Cathodes for Lithium-Ion Batteries with a Ni-Rich Layered Oxide Core and a Li-Rich Layered Oxide Shell. *Adv. Sci.* **2016**, *3* (11), 1600184.
(55) Dogan, F.; Croy, J. R.; Balasubramanian, M.; Slater, M. D.; Iddir, H.; Johnson, C. S.; Vaughey, J. T.; Key, B. Solid State NMR Studies of Li2MnO3 and Li-Rich Cathode Materials: Proton Insertion, Local Structure, and Voltage Fade. *J. Electrochem. Soc.* **2015**, *162* (1), A235−A243.
(56) Ilott, A. J.; Chandrashekar, S.; Klöckner, A.; Chang, H. J.; Trease, N. M.; Grey, C. P.; Greengard, L.; Jerschow, A. Visualizing Skin Effects in Conductors with MRI: 7Li MRI Experiments and Calculations. *J. Magn. Reson.* **2014**, *245*, 143−149.
(57) Muhammad, S.; Kim, H.; Kim, Y.; Kim, D.; Song, J. H.; Yoon, J.; Park, J.-H.; Ahn, S.-J.; Kang, S.-H.; Thackeray, M. M.; Yoon, W.-S. Evidence of Reversible Oxygen Participation in Anomalously High Capacity Li- and Mn-Rich Cathodes for Li-Ion Batteries. *Nano Energy* **2016**, *21*, 172−184.

DOI: 10.1021/acs.chemmater.7b02589
Chem. Mater. 2017, 29, 8282−8291